Eur. Phys. J. D **40**, 57–63 (2006)
DOI: 10.1140/epjd/e2006-00169-0

THE EUROPEAN PHYSICAL JOURNAL D

# On the Stark broadening of $Sr^+$ and $Ba^+$ resonance lines in ultracold neutral plasmas

M.A. Gigosos[1,a], M.Á. González[2], and N. Konjević[3]

[1] Departamento de Óptica, Universidad de Valladolid, 47071 Valladolid, Spain
[2] Departamento de Física Aplicada, Universidad de Valladolid, 47071 Valladolid, Spain
[3] Institute of Physics, P.O. Box 68, 11081 Belgrade, Serbia and Montenegro

Received 12 December 2005 / Received in final form 26 June 2006
Published online 14 July 2006 – 

**Abstract.** We report results of the Stark broadening calculations for $Sr^+$ and $Ba^+$ resonance lines in ultracold plasmas using semiempirical formulas and numerical computer simulation technique. The simulation results show that strong collisions dominate Stark broadening at very low electron temperatures and weak collision approximation used recently by Vrinceanu et al. cannot be applied in this temperature region. Consequently, the temperature trend of Stark widths and shifts changes from $1/\sqrt{T}$ successfully used at elevated temperatures to an increasing trend with temperature, which is characteristic for strong collisions at low temperature.

**PACS.** 32.70.Jz Line shapes, widths, and shifts – 52.70.Kz Optical (ultraviolet, visible, infrared) measurements – 52.65.Yy Molecular dynamics methods

## 1 Introduction

Recently, Vrinceanu et al. [1] have reported results of the electron-impact Stark width and shift calculations for the 421.5 nm $Sr^+$ resonance line in an ultracold neutral plasma. For this purpose the authors [1] used the electron-impact model that follows the one developed by Baranger [2]. This model [2], with several approximations was used successfully at elevated electron temperatures for numerous calculations of the Stark broadening parameters of non-hydrogenic atomic and singly charged ion lines, see e.g. [3]. The authors [1] calculated first the broadening and shift cross-section data in a temperature range 10–200 K, see Figure 1 in [1], and then they used these results to evaluate Stark widths and shifts for the same temperature range and for the electron density $N_e = 10^{16}$ m$^{-3}$. Both, the cross-section data and consequently Stark broadening parameters, show $1/\sqrt{T}$ dependence, see Figures 1 and 2 [1], which suggests very large plasma broadening and shifting of $Sr^+$ resonance lines at $T < 10$ K.

In order to test the possibility of using electron collision models [1,2] for the evaluation of Stark broadening parameters at very low electron temperatures and, in this way, to test their temperature trend, a numerical computer simulation experiment is performed. This approach is also based on a collision model, but in addition to electrons the ion collisions contribution is estimated as well. The basic difference between the two sets of calculations: the computer simulation method is free from numerous approximations involved in the models described in [1,2].

Let us draw attention to some approximations involved in collision model [2]. As can be seen in [2]: "the first is that the perturbers do not interact with each other. Each perturber interacts only with the atom, and is otherwise uncorrelated with the motion of the other perturbers. If we are talking about charged perturbers, this is true only of those that are inside the Debye radius, and we may have to introduce later a correction to take into account the mutual screening of the perturbers" [2]. In this sense, the physical model employed in the calculations [1] and the one used in computer simulations here are identical: perturbers are independent particles that move along straight line trajectories with constant speed according to a Maxwellian velocity distribution corresponding to the temperature of thermal equilibrium. The correlation between charges is taken into account approximately using Debye screened fields. These basic assumptions of the collision model are used in [1,2] and in the computer simulation presented here. The difference between the two sets of calculations comes from the different mathematical treatment of these approximations. The calculation in reference [1] uses the so called "impact approximation", which is a mathematical approximation. The simulation, however, does not use those approximations, and the evolution

[a] e-mail: gigosos@coyanza.opt.cie.uva.es

differential equations are fully integrated. In the analytical calculation [1,2] the Born approximation is used for the development of evolution operator (only the dominant term of the perturbative development of the time evolution operator is taken into account), while in the simulation the differential equations giving the emitter evolution are fully integrated. Further, the analytical development assumes that the collisions do not overlap in time, while in the simulation this must appear in a natural way. It must be remembered that the simulation does not consider "collisions", but it uses the electric field due to the complete set of perturbers. In most time of the simulation, there is not a particle, whose electric field clearly dominates. Only occasionally one particle passes very close to the emitter, and, in those cases, the other particles electric field could be neglected. As will be seen later, these interactions, though very rare, will determine the shift and broadening of the spectral lines studied here. Then, differences between the results of both treatments are not due to differences in the emitter or plasma physical model, but of the mathematical treatment of the interaction between both. To be exact, in the problem considered here, the consideration that have a larger influence on the results is the use of Born approximation: in the usual treatment the phase changes due to the collisions are linear with the intensity of the perturbation; in the simulation this linearity does not appear when we are dealing with close collisions.

In addition, the modified semiempirical formulas [4,5] are also used for the evaluation of $Sr^+$ Stark widths and shifts in a broad temperature range including very low temperatures. These formulas basically use the same theoretical approach [1,2] and the Stark broadening parameters temperature dependence is expected to show the same trend as shown in Figure 2 of reference [1].

All our results for the $Sr^+$ line are compared with those of reference [1] and other experimental data at elevated electron temperatures. In addition the results for the $Ba^+$ 493.4 nm resonance line are reported and discussed.

## 2 Numerical treatment in the simulation

The dipolar emission profile is obtained with the Fourier transform of the emitter dipole moment autocorrelation function [6]:

$$I(\omega) = \frac{1}{\pi}\int_0^\infty \mathrm{d}t \cos(\omega t)\left\{C(t)\right\}, \tag{1}$$

$$C(t) = \mathrm{tr}\left[\mathbf{D}(t)\cdot\mathbf{D}(0)\right], \tag{2}$$

$$\mathbf{D}(t) = U^+(t)\mathbf{D}(0)U(t), \tag{3}$$

where $\mathbf{D}$ is the dipole moment of the transition under study — normalized so that $C(0) = 1$ — and $U(t)$ is the time evolution operator of the system, that obeys the Schrödinger equation:

$$\mathrm{i}\hbar\frac{\mathrm{d}}{\mathrm{d}t}U(t) = \left[H_0 + q\mathbf{E}(t)\cdot\mathbf{R}\right]U(t). \tag{4}$$

$H_0$ is the unperturbed emitter Hamiltonian, $\mathbf{E}(t)$ is the electric field sequence undergone by the emitter, and $q\mathbf{R}$ is its dipole moment. In our calculations we have not considered the *no-quenching* approximation, so that operator $\mathbf{R}$ and $\mathbf{D}$ are proportional.

In a computer simulation the perturbers — ions and electrons — behaviour is reproduced numerically, and the electric microfield $\mathbf{E}$ at the emitter position is calculated. Once this field is evaluated, the equations (4) are solved numerically and by using equation (3) the evolution of dipole moment is obtained. This calculation is repeated a large number of times with a representative set of microfield temporal sequences. In expression (1) symbols $\{\ \}$ mean an average of emitters in the plasma, what in our case means an average of the emitter dipole autocorrelation functions, each of them obtained from a sequence of the perturber microfield $\mathbf{E}(t)$. The details how particles are generated in the simulation, including the reinjection technique are described in reference [7].

The correlations between charged particles will be approximated here as in [7,8], using a plasma model of non interacting particles, under thermal equilibrium, with Debye screened fields. For some of the conditions considered in the simulation (low temperature and high density) the plasma coupling parameter is a large number characteristic for non ideal plasma. In these cases it would be necessary to perform a study of the interactions between particles using a molecular dynamics simulation technique. Since the aim of this work was not to provide quantitative data for comparison with experimental results, but to study the influence of temperature within the frame of the physical model used in [1] (independent particles with a screening correction to emulate the correlations), then in order to take into account correlations in the simulations only a screening correction for independent particles is used. In this sense, strongly coupled plasma cases may be considered as an extrapolation. In fact, when one takes into account the correlation between particles the collisions efficiency is reduced and the values of width and shift decrease as well [8]. This effect will contribute to the decrease of width and shift with decreasing temperature.

In the computer simulation, the perturbers movement and the emitter evolution are carried on with discrete *time steps* $\Delta t$. These steps are chosen so that the electric field $\mathbf{E}(t)$ may be considered static for the time duration of the step. In this case, the solution of the differential equation (4) is:

$$\begin{aligned} U(t+\Delta t) &= M(t+\Delta t, t)U(t) \\ &\simeq \exp\left[-\frac{\mathrm{i}}{\hbar}\left(H_0 + q\mathbf{E}(t)\cdot\mathbf{R}\right)\Delta t\right]U(t). \end{aligned} \tag{5}$$

To calculate this exponential, it is necessary to obtain the eigenvalues and the eigenvectors of the Hamiltonian. Therefore, it is convenient to rewrite that Hamiltonian in the following way

$$H(t) = \mathcal{R}^{-1}(\theta,\varphi)\left[H_0 + qE(t)R_z\right]\mathcal{R}(\theta,\varphi) \tag{6}$$

where

$$\mathcal{R}(\theta,\varphi) = e^{-\mathrm{i}J_y\theta}e^{-\mathrm{i}J_z\varphi} \tag{7}$$

is the rotation matrix that turns the operator $\mathbf{E}(t)\cdot\mathbf{R}$ to $E(t)R_z$. Angles $\theta(t)$ and $\varphi(t)$ are the electric field vector polar angles, while $E(t)$ is its module:

$$\mathbf{E} = (E\sin\theta\cos\varphi, E\sin\theta\sin\varphi, E\cos\theta). \tag{8}$$

The numerical process to be programmed is the diagonalization of the matrix that appears in equation (6), with the electric field oriented always along the $Z$-axis. We use the standard spherical basis $|n,l,j,m_j\rangle$, where the matrix $H_0$ is diagonal and the matrix $R_z$, with all real elements, connects only states with the same value of $m_j$. We can then organize the calculation with boxes having fixed value of $m_j$. The Hamiltonian is then prepared as a matrix with six diagonal boxes, each one belonging to one of the values $m_j = \pm 5/2$, $\pm 3/2$ and $\pm 1/2$ with dimensions 1, 3 and 6, respectively. Here is used the Jacobi method for the numerical diagonalization [11], which is very convenient for small matrixes. This method allows us to obtain simultaneously the eigenvalues and the matrix $Q$ that gives the change to diagonal shape. We now have

$$H_0 + qE(t)R_z = Q^t H_D(t) Q \tag{9}$$

where $H_D$ is diagonal.

In standard basis $|n,l,j,m_j\rangle$ the matrix $J_z$ is diagonal and each element of $J_y$ is pure imaginary, so that the matrix $\mathcal{R}(\theta,\varphi)$ is formed by the product of a real and a — complex — diagonal matrix:

$$\langle n'l'j'm'_j|\mathcal{R}(\theta,\varphi)|nljm_j\rangle = \delta_{j'j} d^j_{m'_j m_j}(\theta) e^{-\mathrm{i}m_j\varphi} \tag{10}$$

with $d^j_{m'_j m_j}(\theta) = \langle j,m'|e^{-\mathrm{i}J_y\theta}|jm\rangle$ (see notation in [12]).

For each time step one gets the numerical expression of matrix $M(t+\Delta t,t)$ — see expression (5) — and it is then multiplied by $U(t)$ to go to next time step.

Once the evolution operator $U(t)$ is obtained, the dipole autocorrelation function must be calculated — expressions (2) and (3) —. During the numerical calculation it is convenient to extract the frequencies corresponding to the energies of the unperturbed states from the system evolution. For this purpose the evolution operator may be written as

$$U(t) \equiv \exp\left[-\frac{\mathrm{i}}{\hbar}H_0 t\right]\tilde{U}(t) \tag{11}$$

with a diagonal matrix $H_0$. In this expression, the matrix $\tilde{U}(t)$ accounts of the "*modulation*" in the evolution of the emitter states caused by the perturbations. In general we are interested here in configurations with perturbations that give rise to "*modulations*" of very low frequency in comparison with the optical transitions frequencies. They correspond, then, to lines with very weak Stark broadening.

With this notation, the autocorrelation function may be written as:

$$\begin{aligned} C(t) &= \mathsf{tr}\left[\tilde{U}^+(t)e^{+\frac{\mathrm{i}}{\hbar}H_0 t}\mathbf{D}e^{-\frac{\mathrm{i}}{\hbar}H_0 t}\tilde{U}(t)\cdot\mathbf{D}\right] \\ &= \mathsf{tr}\left[e^{+\frac{\mathrm{i}}{\hbar}H_0 t}\mathbf{D}e^{-\frac{\mathrm{i}}{\hbar}H_0 t}\cdot\tilde{U}(t)\mathbf{D}\tilde{U}^+(t)\right]. \end{aligned} \tag{12}$$

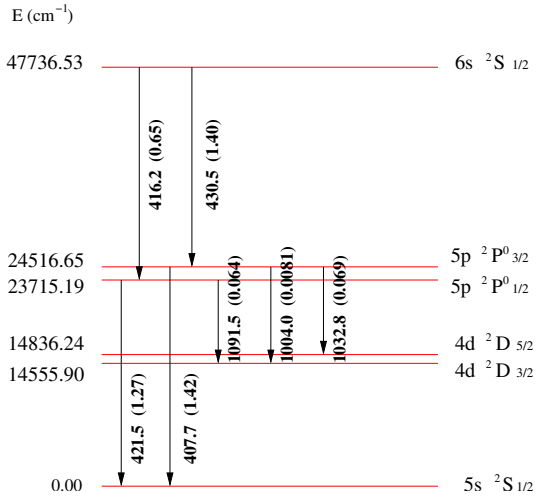


**Fig. 1.** Grotrian diagram for the $Sr^+$ transitions used for the computer simulation experiments. For each transition, wavelength (in nm units) and transition probability (in brackets, in $10^8$ s$^{-1}$ units) are given. Wavelengths and transition probabilities were taken from references [9,10].

By expressing the autocorrelation function in this way the separation of both domains of frequencies is possible. The matrix $e^{+\frac{\mathrm{i}}{\hbar}H_0 t}\mathbf{D}e^{-\frac{\mathrm{i}}{\hbar}H_0 t}$ takes into account the high frequency component of the function $C(t)$, which corresponds to the frequency of the optical transitions. This is a fixed matrix function that does not depend on the perturber field. The other matrix, $\tilde{U}(t)\mathbf{D}\tilde{U}^+(t)$, takes account of the — low frequency — modulations induced by the perturbations. It is convenient to follow this frequency separation in the computer, so that numerical errors can be reduced as much as possible.

The energy states connected through matrixes $\mathbf{D}$ are shown in Figure 1. The elements of these matrixes are functions with the shape $D_{ij}e^{\mathrm{i}\omega_{ij}t}$. In the system under study seven transitions, see Figure 1, are taken into account, so one can write

$$e^{+\frac{\mathrm{i}}{\hbar}H_0 t}\mathbf{D}e^{-\frac{\mathrm{i}}{\hbar}H_0 t} \equiv \sum_{k=1}^{7}\left[e^{\mathrm{i}\omega_k t}\mathbf{D}_k + e^{-\mathrm{i}\omega_k t}\mathbf{D}_k^+\right] \tag{13}$$

where $\mathbf{D}_k$ (or $\mathbf{D}_k^+$) is the part of the matrix $\mathbf{D}$ that connects the states whose difference in energies is $\hbar\omega_k$ (or $-\hbar\omega_k$). This development may be translated to the autocorrelation function in the following way:

$$\begin{aligned} C(t) &= \sum_{k=1}^{7}\mathsf{tr}\left[\left(e^{\mathrm{i}\omega_k t}\mathbf{D}_k + e^{-\mathrm{i}\omega_k t}\mathbf{D}_k^+\right)\cdot\tilde{U}(t)\mathbf{D}\tilde{U}^+(t)\right] \\ &= \sum_{k=1}^{7}\cos(\omega_k t)C_k^c(t) - \sin(\omega_k t)C_k^s(t), \end{aligned} \tag{14}$$

where

$$C_k^c(t) \equiv \mathsf{tr}\left[\left(\mathbf{D}_k + \mathbf{D}_k^+\right)\cdot\tilde{U}(t)\mathbf{D}\tilde{U}^+(t)\right], \tag{15}$$

$$C_k^s(t) \equiv \mathsf{tr}\left[\frac{1}{\mathrm{i}}\left(\mathbf{D}_k - \mathbf{D}_k^+\right)\cdot\tilde{U}(t)\mathbf{D}\tilde{U}^+(t)\right]. \tag{16}$$

(Both quantities $C_k^c(t)$ and $C_k^s(t)$ are real numbers.) In order to calculate the line profile the above expressions are introduced in equation (1):

$$I(\omega) = \sum_{k=1}^{7} \frac{1}{\pi} \int_0^\infty \mathrm{d}t \cos(\omega t) \left\{ \cos(\omega_k t) C_k^c(t) - \sin(\omega_k t) C_k^s(t) \right\}. \quad (17)$$

The development of the products

$$\cos(\omega t) \cos(\omega_k t)$$

and

$$\cos(\omega t) \sin(\omega_k t)$$

gives rise to terms in $\cos((\omega - \omega_k)t)$ and $\cos((\omega + \omega_k)t)$ as well as $\sin((\omega - \omega_k)t)$ and $\sin((\omega + \omega_k)t)$. Terms in $(\omega + \omega_k)$ take account of frequencies that do not appear in the correlation functions $C_k^c(t)$ and $C_k^s(t)$. These are slow varying functions in time so they can be disregarded. In this way,

$$I(\omega) = \sum_{k=1}^{7} \frac{1}{\pi} \int_0^\infty \mathrm{d}t \big[ \cos((\omega - \omega_k)t) \{C_k^c(t)\} + \sin((\omega - \omega_k)t) \{C_k^s(t)\} \big], \quad (18)$$

corresponds to the profiles of seven possible $Sr^+$ spectral lines, see Figure 1.

## 3 Simulation results

Before we start the discussion of the results it should be noted that a simulation at an electron density of $N_e = 10^{16}$ m$^{-3}$ and $T = 100$ K requires a huge computation time as a consequence of the very small Stark broadening. This is the reason why the electron density and temperature have been scaled so that our central conditions ($N_e = 10^{23}$ m$^{-3}$, $T = 21539$ K) correspond to a plasma with the same coupling parameter as the one in [1]. This extrapolation will be discussed and justified in relation to the reported results.

Figure 2b shows a typical example of the dipole autocorrelation function corresponding to the electric field sequence shown in Figure 2a. Under weak field conditions, the correlation loss is very slow. When a strong collision takes place the emitter dipole suddenly looses coherence with a "*step*" function shape. The height of this step depends upon the integral of energy transfer between the perturber and the emitter atom. It should be noticed that when the energy — expressed as a phase of the evolution operator — is significant, the relationship between the perturber field and the phase step is not linear. For very strong collisions a monotonous relationship between the phase change and the perturbation magnitude is not necessarily expected, i.e. this is a total coherence breakdown situation. When one considers very weak collisions,

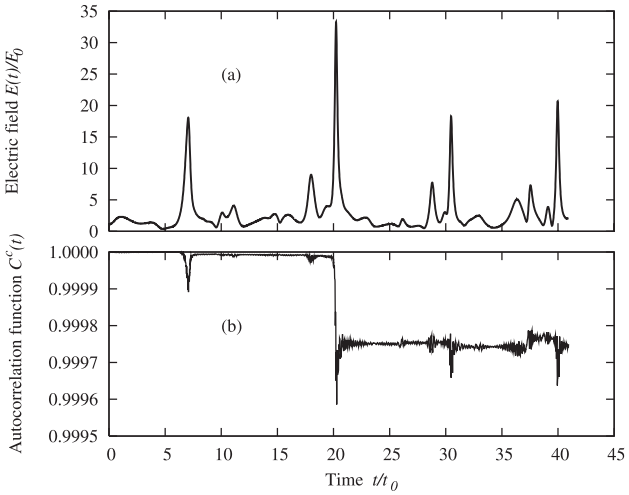


**Fig. 2.** An example of calculated electric field and autocorrelation function: (a) a typical time sequence of the electric field modulus; (b) the corresponding emitter dipole autocorrelation function $C^c(t)$. The function $C^c(t)$ under weak collisions conditions decreases very slowly. Only when a strong collision occurs a noticeable change in the correlation function is detected. In this example, though the electric field sequence were canceled except around $t \approx 20t_0$, the correlation loss at $t \approx 40t_0$ would have been the same. In this figure, and in Figure 3, $t_0 = r_0/v_0$, $r_0 = (4\pi N_e/3)^{-1/3}$, $v_0 = \sqrt{2kT/m_e}$ and $E_0 = q_e/(4\pi\epsilon_0 r_0^2)$.

the relationship between the phase change and the perturbation energy is linear and the so called impact approximation has physical meaning: non overlapping weak collisions with very short duration. This approximation leads to the width and shift dependence upon electron density and temperature, which after simplification of some details scales the line width with $N_e/\sqrt{T}$ [1,2]. Strong collisions however establish a relationship more similar to $\sim N_e\sqrt{T}$. Namely, very strong collisions give rise to sudden changes of the phase — the "*steps*" — whose magnitude hardly depends on the density and the temperature. The frequency of those collisions, however, is proportional to $N_e\sqrt{T}$. When weak collisions are very weak, their effect is masked by strong collisions, which dominate line broadening. This is exactly what is happening here for the studied transition, see Figures 2 or 3. Therefore, we can conclude here from the simulations results that the Sr II 421.5 nm line Stark profile is dominated by strong collisions.

Computer simulation permits testing to what extent the strong collisions are the dominant collisions. To achieve this goal, we performed a computer simulation in which the electric microfield sequences were modified according to

$$\mathbf{E}'(t) = \begin{cases} \mathbf{E}(t) & \text{if } E(t) = |\mathbf{E}(t)| \le E_{max}, \\ E_{max} \dfrac{\mathbf{E}(t)}{E(t)} & \text{if } E(t) > E_{max}. \end{cases} \quad (19)$$

This means that we truncated the perturber field modulus to a pre-established value $E_{max}$ but we kept its orientation. The results in Table 1 represent several examples obtained in these calculations. If the collisions with

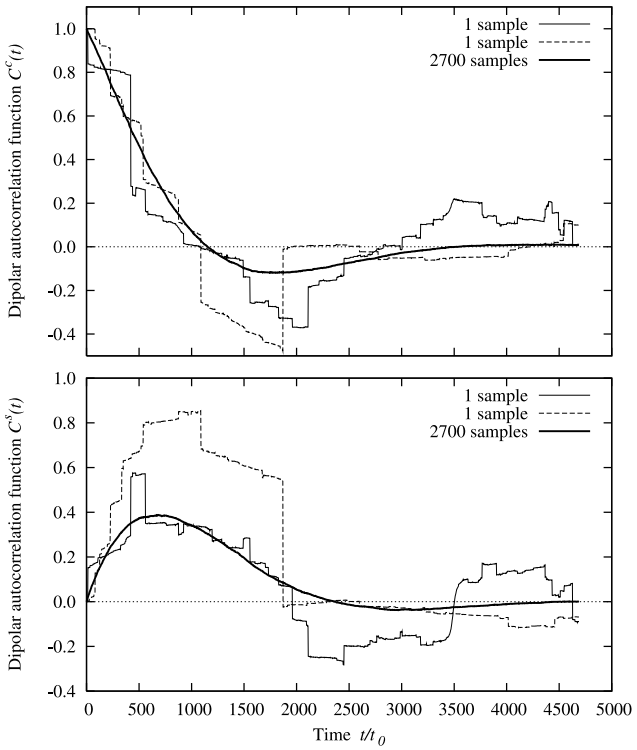


**Fig. 3.** Cosine and sine parts of the emitter dipole autocorrelation function for the 421.5 nm $Sr^+$ line for one of the cases considered in this work ($N_e = 10^{23}$ m$^{-3}$, $T = 21539$ K). Two typical examples are shown, each of them is obtained with only one microfield sample, — the same field temporal sequence for the functions $C^s(t)$ and $C^c(t)$ — together with the final result obtained with 2700 samples. The autocorrelation functions have the shape of step functions, with steps lengths corresponding to the times of very strong collisions.

**Table 1.** Total width and shift of the 421.5 nm Sr II line obtained in the simulation experiment with the electric field truncated to $E_{max}$. In these calculations, only the field due to electrons is considered ($N_e = 10^{23}$ m$^{-3}$, $T = 21539$ K). The field $E_0$ is the normal field strength corresponding to the stated electron density. The last column shows (in %) the time fraction when the original field has a modulus larger than $E_{max}$.

| Electrons only with truncated field | | | |
|---|---|---|---|
| $E_{max}(E_0)$ | FWHM (GHz) | shift (GHz) | % collisions |
| $\infty$ | 103.7 | 69.3 | 0.000 |
| 100 | 5.00 | 34.0 | 0.096 |
| 50 | 1.40 | 23.2 | 0.290 |

electric fields larger than one hundred times the normal field strength are eliminated, the total width is reduced to ≈5%, see Table 1. These collisions correspond only to a 0.096% of the total simulation time. The field larger than $100E_0$ corresponds to collisions with an impact parameters lower than $0.1r_0$, what corresponds to 1.33 nm in the considered example.

It is well-known, that the domain of strong collisions may be characterized by the Weisskopf radius [13], $r_w$, which is defined as the distance below which the individual collisions are able to produce a change of phase

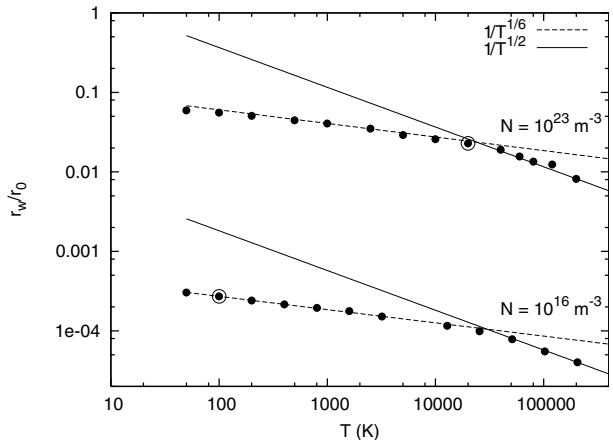


**Fig. 4.** Weisskopf radius as a function of temperature for two electron density conditions. The value of $r_w$ has been fixed as the impact parameter of an individual collision that gives rise to a change equal to one in the emitter dipole autocorrelation function. The values corresponding to the central conditions of the simulation study and those in [1] are marked in this figure with an additional circle. In both cases marked circles are in a region where the dependence of the Weisskopf radius upon temperature is much weaker than $1/\sqrt{T}$. For the low density case this situation is more clear than for the high density one. When the Weisskopf radius decreases with a trend weaker than $1/T^{1/4}$ the width induced by strong collisions will have growing trend with temperature. This comes as a consequence of strong collisions frequency, which is proportional to $\sqrt{T}$.

greater than $\pi$ in the evolution of the emitter dipole. Using this criterion in reference [13] it is estimated that the line broadening due to strong collisions follows a trend proportional to $N_e\sqrt{T}r_w^2$. The numerical treatment employed here permits the evaluation of the Weisskopf radius for our work conditions. In order to achieve this goal the emitter dipole autocorrelation function was calculated for an individual collision between an electron and an emitter atom using a straight trajectory and mean square velocity $v_0 = \sqrt{2kT/m_e}$. We have taken as the Weisskopf radius the impact parameter that must be chosen in such a way that the *step* produced in $C^c(t)$ is equal to one — see exp. (15) —. This means that $C^c(t)$ passes from $C^c(-\infty) = 1$ to $C^c(+\infty) = 0$. Figure 4 shows calculated values of the Weisskopf radius for two electron densities: the one used here ($N_e = 10^{23}$ m$^{-3}$), and the lower one used in reference [1] ($N_e = 10^{16}$ m$^{-3}$). It is important to notice that low density results do not represent results of a linear re-scaling of the high density ones. The Weisskopf radius calculations were performed at the pointed densities and temperatures. It must be taken into account that these calculations were done with a simulation of a single collision, so they are affordable cases in the simulation. In fact, they were obtained considering in the simulation time steps much smaller than those considered in the usual simulation calculations. Both sets of results in Figure 4 show a temperature dependence that, in the domain analysis, do not correspond to the trend $r_w \sim 1/\sqrt{T}$, which would produce an increase of the spectral line width as temperature

decreases. One has to select very high temperatures to find a strongly decreasing trend with the temperature.

It is known that the Weisskopf radius does not depend on electron density and it is only a parameter-indicator when a collision is strong enough to produce a change of phase equal to one. Thus Figure 4 shows only that at low density ($r_0$ is, then, larger) the Weisskopf radius is much smaller than the mean interparticle distance. This means that "strong collisions" are relatively less frequent. Here we must return to Figure 2, which shows that the only significant correlation loss for this example, is the one induced by the peak at $t \approx 20t_0$. Although we would have completely gone without the rest of the electric field, the correlation loss would have been the same. This phenomenon appears when the average collision is very weak. It's more, the weaker the typical collision were, the more noticeable this effect would be. In this sense our extrapolation to low density is completely justified. When density is reduced, the ratio between the Weisskopf radius and the mean interparticle distance becomes smaller. Then, strong collisions are less probable, but, we want to point out that outside the Weisskopf radius collisions have negligeable effect in comparison to those of the few strong collisions. If one would expect that the dependence of the line width with temperature be of the type $1/\sqrt{T}$, Weisskopf radius at low densities should recover the trend $1/\sqrt{T}$ at low temperatures. This effect has not been observed in the simulation experiments. The trend $1/\sqrt{T}$ of Weisskopf radius only appears for temperatures over 20 000 K. This observation justifies, once more, the extrapolation of our calculations at low densities.

The simulation results are shown in Figure 5 together with corresponding data from Modified Semiempirical Formulas [4,5], available experimental values [14–16] and calculated ones from Figure 2 of reference [1]. Critical evaluations and uncertainty estimation of $Sr^+$ and $Ba^+$ experimental data are given in references [17,18]. In any case, the range in temperatures covered by the available experiments as well as their uncertainty do not permit to know experimentally the dependences of line width and shift with temperature. For the electron density scaling of all the data in Figures 5 to 7 the linear dependence of the Stark width and shift is assumed. The same assumption is used to scale up data from Vrinceanu et al. [1], corresponding to an electron density of $N_e = 10^{16}$ m$^{-3}$. These extrapolations are justified in both models, [1] and in our simulations, — see Figure 6 —. Since linear dependence of Stark width upon electron density is an important issue here, where data at very different electron densities are compared, a short discussion of this subject will be carried out. It is important to notice that in the treatment of both, very weak and very strong collisions, the dependence of the width upon the electron density is linear. For the first case — very weak collisions — the linearity appears because the perturber field correlation is lost much earlier than the emitter dipole autocorrelation, and the broadening process becomes homogeneous in time. In the second case — very strong collisions — the linearity appears because these collisions never overlap in time — binary approximation is always valid — and two consecutive collisions are statistically independent. In both cases, the simulation results show a linear dependence upon electron concentration for medium densities while at very low densities this dependence can be much easier proven. The proof of the Stark broadening parameters linear dependence upon electron density justifies, a posteriori, our calculations, which were done at much higher density than in [1].

The most important result of the computer simulations is the temperature trend of the line width and shift, which

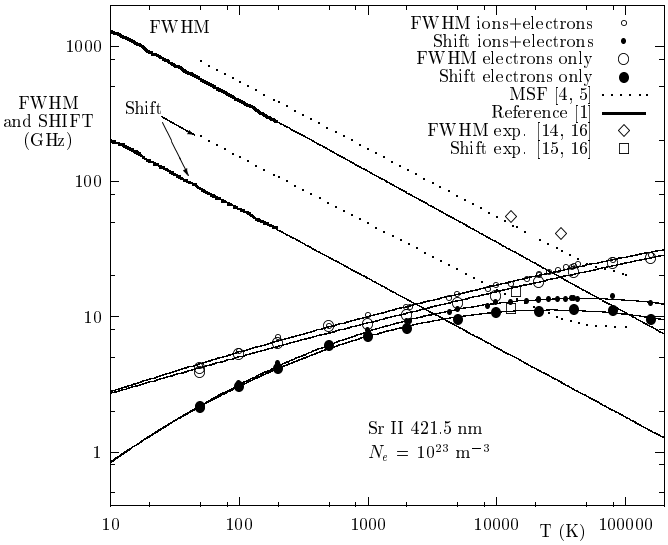


**Fig. 5.** Total width at half maximum (FWHM) and shift of the 421.5 nm Sr II line. The simulation results for the joint broadening of electrons and ions at $N_e = 10^{23}$ m$^{-3}$ are presented with empty circles, while full circles are used for electrons only broadening. Thin lines show best fit of the simulation results. Results corresponding to the Modified Semiempirical Formulas (MSF [4,5], dotted line) and those appearing in Figure 2 of [1] (continuous thick line) are also shown. Thin line represents temperature extrapolation of data [1] using $1/\sqrt{T}$ relation.

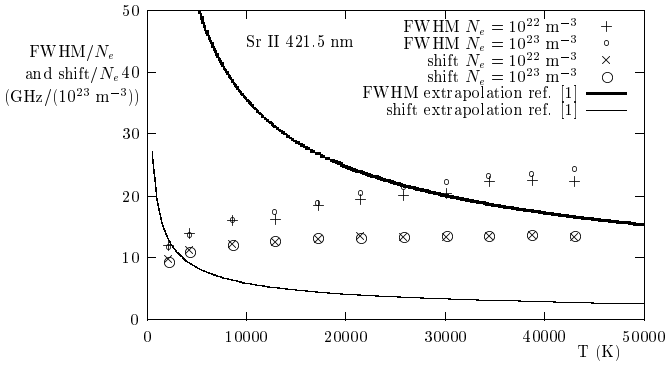


**Fig. 6.** Full width at half maximum and line shift of the 421.5 nm Sr II line normalized to the electron density. The simulation results show an increasing trend of both width and shift with the electron temperature. The extrapolated results of reference [1] in the same temperature range are also shown in this figure.

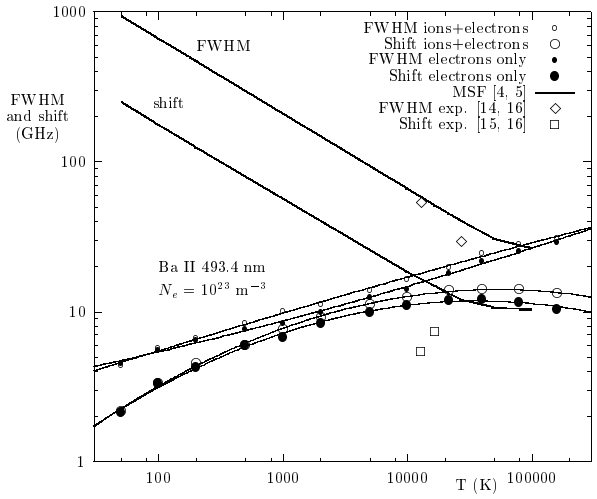


**Fig. 7.** Same as in Figure 5 but for the 493.4 nm Ba II line.

is quite different from the one predicted by the model used in [1]. As expected, the results of Modified Semiempirical Formulas [4,5] show the same trend as shown in [1]. The origin of both approaches [1,4,5] is the same and starts from reference [2].

The simulation results corresponding to the calculations with joined effect of ions and electrons are compared with other theoretical results considering only electron collisions, see Figure 5. For the studied cases, the ionic fields are responsible for a little less than 10% of the total width and shift.

Likewise, computer simulations were carried on for the 493.4 nm Ba II line. The level structure in this case is similar to that of the Sr II. The results are shown in Figure 7 together with experimental data and results of the Modified Semiempirical Formula. The observed trends, both for the width and the shift, are similar to those found for the Sr II.

## 4 Conclusions

The aim of this work is not to supply accurate values of $Sr^+$ and $Ba^+$ line widths and shifts for quantitative comparison with experiment. This would require to use Molecular Dynamics simulations of interacting particles with consideration of the emitter charge. It is not expected however that these results would differ qualitatively from those presented here.

The most important result of this work is an indication that strong collisions dominate Stark broadening at very low electron temperatures and therefore the theoretical approaches based on weak collisions assumption, see e.g. [2], cannot be applied in this temperature region. Consequently the temperature trend of Stark widths and shifts changes from $1/\sqrt{T}$ used at elevated temperatures to an increasing trend with temperature, which is characteristic of strong collision cases [6]. Our results in Figures 5, 6 and 7 indicate that width and shift have a increasing dependence with an increase of the temperature and suggest that Stark broadening in ultracold plasmas at relatively low electron densities $N_e < 10^{16}$ m$^{-3}$ is negligible. In favor of this conclusion speaks also an experimental fact: the generation and confinement of ultracold plasmas at very low temperatures would be followed by a huge drift of the optimal laser→plasma interaction wavelength if the Stark shift do no comply temperature dependence of the simulation results, see Figures 5 to 7. Namely, the wavelength of Sr II and Ba II resonance lines are used for laser trapping and cooling of strontium and barium ultracold plasmas. To the authors knowledge such systematic and large shifts of the optimum pumping laser wavelength are not detected even for very low temperatures.

This work has been partially supported by the Spanish Ministerio de Educación y Ciencia under grants FTN2001-1827 and ENE2004-05038/FTN. The support of the Ministry of Science and Environment Protection of the Republic of Serbia is also acknowledged.

## References

1. D. Vrinceanu, H.R. Sadeghpour, K. Bartschat, J. Phys. B: At. Mol. Opt. Phys. **37**, L371 (2004)
2. M. Baranger, Phys. Rev. **111**, 481 (1958)
3. H.R. Griem, *Spectral Line Broadening by Plasmas* (Academic Press, New York and London, 1974)
4. M.S. Dimitrijević, N. Konjević, J. Quant. Spectrosc. Radiat. Transfer **24**, 451 (1980)
5. M.S. Dimitrijević, N.V. Kršljanin, Astron. & Astrophys. **165**, 269 (1986)
6. P.W. Anderson, Phys. Rev. **76**, 647 (1949)
7. M.A. Gigosos, V. Cardeñoso, J. Phys. B: At. Mol. Opt. Phys. **29**, 4795 (1996)
8. E. Dufour, A. Calisti, B. Talin, M.A. Gigosos, M.Á. González, T. del Río Gaztelurrutia, J.W. Dufty, Phys. Rev. E **71**, 066409-1 (2005)
9. `http://physics.nist.gov/PhysRefData/ASD/index.html`
10. `http://cfa-www.harvard.edu/amdata/ampdata/kurucz23/sekur.html`
11. W.W. Press, S.A. Teukolsky, W.T. Vetterling, B.P. Flannery, *Numerical Recipes un C* (Cambridge University Press, New York, 1997)
12. L.C. Biedenharn, J.D. Louck, *Angular Momentum in Quantum Physics* (Addison-Wesley Pub, 1981)
13. H. Margenau, M. Lewis, Rev. Mod. Phys. **31**, 569 (1959)
14. D. Hadžiomerspahić, M. Platiša, N. Konjević, M. Popović, Z. Phys. **262**, 262 (1973)
15. J. Purić, N. Konjević, Z. Phys. **249**, 440 (1972)
16. C. Fleurier, S. Sahal-Brechot, J. Chapelle, J. Quant. Spectrosc. Radiat. Transfer **17**, 595 (1977)
17. N. Konjević, W.L. Wiese, J. Phys. Chem. Ref. Data **5**, 259 (1976)
18. N. Konjević, M.S. Dimitrijević, W.L. Wiese, J. Phys. Chem. Ref. Data **13**, 649 (1984)